Current Alzheimer Research, 2020, *17*, 1145-1160

RESEARCH ARTICLE

Diagnosis of Mild Cognitive Impairment Using Cognitive Tasks: A Functional Near-Infrared Spectroscopy Study

So-Hyeon Yoo[1], Seong-Woo Woo[1], Myung-Jun Shin[2], Jin A. Yoon[2], Yong-Il Shin[3] and Keum-Shik Hong[1,4,*]

[1]*School of Mechanical Engineering, Pusan National University, 2 Busandaehak-ro, Geumjeong-gu, Busan 46241, Republic of Korea;* [2]*Department of Rehabilitation Medicine, Pusan National University School of Medicine and Biomedical Research Institute, Pusan National University Hospital, Busan 46241, Republic of Korea;* [3]*Department of Rehabilitation Medicine, Pusan National University School of Medicine, Pusan National University Yangsan Hospital, Yangsan 50612, Republic of Korea;* [4]*Department of Cogno-Mechatronics Engineering, Pusan National University, 2 Busandaehak-ro, Geumjeong-gu, Busan 46241, Republic of Korea*

Abstract: ***Background*:** Early diagnosis of Alzheimer's disease (AD) is essential in preventing its progression to dementia. Mild cognitive impairment (MCI) can be indicative of early-stage AD. In this study, we propose a channel-wise feature extraction method of functional near-infrared spectroscopy (fNIRS) data to diagnose MCI when performing cognitive tasks, including two-back, Stroop, and semantic verbal fluency tasks (SVFT).

***Methods*:** A new channel-wise feature extraction method is proposed as follows: A region-of-interest (ROI) channel is defined as such channel having a statistical difference ($p < 0.05$) in *t*-values between two groups. For each ROI channel, features (the mean, slope, skewness, kurtosis, and peak value of oxy- and deoxy-hemoglobin) are extracted. The extracted features for the two classes (MCI, HC) are classified using the linear discriminant analysis (LDA) and support vector machine (SVM). Finally, the classifiers are validated using the area under curve (AUC) of the receiver operating characteristics. Furthermore, the suggested feature extraction method is compared with the conventional approach. Fifteen MCI patients and fifteen healthy controls (HCs) participated in the study.

***Results*:** In the two-back and Stroop tasks, HCs showed activation in the ventrolateral prefrontal cortex (VLPFC). However, in the case of MCI, the VLPFC was not activated. Instead, Ch. 30 was activated. In the SVFT task, the PFC was activated in both groups, but the *t*-values of HCs were higher than those of MCI. For the SVFT, the classification accuracies using the proposed feature extraction method were 80.77% (LDA) and 83.33% (SVM), showing the highest among the three tasks; for the Stroop task, 79.49% (LDA) and 73.08% (SVM); and for the two-back task, 73.08% (LDA) and 69.23% (SVM).

***Conclusion*:** The cognitive disparities between the MCI and HC groups were detected in the ventrolateral prefrontal cortex using fNIRS. The proposed feature extraction method has shown an improvement in the classification accuracies, see Subsection 3.3. Most of all, the suggested method contains a group-distinction information per cognitive task. The obtained results successfully discriminated MCI patients from HCs, which reflects that the proposed method is an efficient tool to extract features in fNIRS signals.

ARTICLE HISTORY

Received: April 30, 2020
Revised: October 18, 2020
Accepted: December 22, 2020

DOI:
10.2174/1567205018666210212154941

Keywords: Mild cognitive impairment (MCI), functional near-infrared spectroscopy (fNIRS), semantic verbal fluency task (SVFT), feature selection, linear discriminant analysis (LDA), Alzheimer's disease.

1. INTRODUCTION

Alzheimer's disease (AD) is the most common progressive neurodegenerative brain disease characterized by a gradual deterioration in cognitive function [1]. Generally, patients with AD exhibit various impairments during everyday tasks, such as difficulties in word-finding, spatial cognition, highly altered episodic memory, and executive functions, as well as neuropsychiatric changes [2]. An official report indicated that about 5.7 million Americans have AD [3], and 11,561 people died of AD in the United States in 2018. AD is the fifth leading reason of death for Americans aged over 65 years. The healthcare costs for patients with AD are expected to increase rapidly in the coming years because of the aging population. Many studies revealed that the effective treatment of drugs and routine training could

*Address correspondence to this author at the School of Mechanical Engineering, Pusan National University, Busan 46241, Korea; Tel: +82-51-510-2454; Fax: +82-51-514-0685; Email: kshong@pusan.ac.kr

1875-5828/20 $65.00+.00

delay disease progression and thus enhance the quality of life for patients with AD [4, 5]. However, early diagnosis of AD is clinically crucial because the disease has already progressed a lot by the time when pathological symptoms of AD become apparent. Therefore, after diagnosing MCI, treatment to delay AD progression should start as early as possible. Many researchers have searched for possible features/biomarkers of AD that could enable early detection of AD, such as deposition of the amyloid-beta peptide [6], the presence of tau proteins, and the tangle of nerve fibers with neuronal loss in neurotransmitter systems [7]. In this study, we develop a diagnostic method for early detection of MCI, in which the cognitive abilities of aged people are measured with the use of functional near-infrared spectroscopy (fNIRS).

MCI is known to represent an early stage of dementia. It is a disorder in the intermediate state that exhibits a more rapid cognitive decline than that can be seen during normal aging [8]. Clinically, the possibility of progression from MCI to AD occurs within 5 years, which is shorter than that in the normal elderly [9]. Therefore, early diagnosis of MCI can serve as an important factor in delaying or preventing the onset of AD. Clinical diagnosis of MCI is made by examining the history of a patient's behavior obtained from the patient's caregiver and/or the results from neuropsychological examinations such as the Mini-Mental State Examination (MMSE) [10, 11]. However, the variability of clinical evaluations (due to the experimenter's manual inputs and interpretation) requires experienced clinical professionals and a thorough clinical examination design, which results in additional medical costs, as well as the presence of subjectivity and variability of diagnostic results. To compensate for the limitations of these neuropsychological examination methods, the developed quantitative approaches to diagnose MCI include invasive methods, such as the collection and analysis of cerebrospinal fluid (CSF) [12-14], which is a common biomarker for AD, and non-invasive brain imaging techniques, such as magnetic resonance imaging (MRI) [15], positron emission tomography (PET) [16], magnetoencephalography (MEG) [17, 18], and electroencephalography (EEG) [19]. However, CSF examination requires a lumbar puncture, whereby a long needle is inserted into the spinal cord. Presently, MRI is commonly used to visualize the brain structure of patients with MCI (*e.g.*, to measure the volume of the hippocampus and atrophy of the hippocampal pathway) [20, 21] and to identify task-relevant functional brain connectivity [22-24]. Additionally, functional MRI (fMRI) has been used to image the changes in brain activity over time. PET imaging has also been used to investigate the brain metabolic system of patients with MCI and to visualize the deposition of amyloid-beta [25-29]. However, MRI and PET cannot be repeatedly used for clinical purposes owing to the strict measurement requirements, device size, low temporal resolution, motion artifacts, high cost, and potential harm to the brain [30]. EEG has also been used in MCI research by recording electric signals that are propagated from activated neuron populations (*i.e.*, alpha, beta, and delta waves) [20, 31]. People with MCI have been found to have different functional connectivity [32], frequency relative power [33], and event-related potentials (ERPs) [34] compared to those of age-matched healthy controls. EEG has a high temporal resolution, and the apparatus can be portable. However, it has a limited spatial resolution, and its signals are often contaminated by electrical devices (environmental artefacts) and motion artefacts [35]. CSF, MRI, and PET are not suitable for periodic checkups, limiting the ability to track the course of the disease [30], and the EEG data for MCI diagnosis are not conclusive yet.

Recently, fNIRS has been widely used to image brain functions [36]; it uses more than two near-infrared wavelengths to measure the concentration changes of oxy-hemoglobin (ΔHbO) and deoxy-hemoglobin (ΔHbR) associated with the metabolic activity of neurons in the cerebral cortex. Compared with MRI and PET, fNIRS is known for its high temporal resolution, mobility, low cost, low susceptibility to motion artefacts, safety, and less restriction of the subjects to remain constrained during experiments (like fMRI). fNIRS also has a better spatial resolution than EEG and can provide functional imaging by measuring the cerebral cortical hemodynamic responses (HRs). Thus, fNIRS has the potential to be an alternative to fMRI [37] once the number of channels is increased.

Recently, researchers have investigated whether the HRs between healthy controls (HCs) and the patients with MCI using fNIRS can be compared or not [38-40]. Previous fNIRS studies have demonstrated that brain activities can be measured during various tasks, including working memory tasks [41-43], memory encoding tasks [44, 45], Stroop task [46], and verbal fluency tasks [47, 48]. Furthermore, connectivity analysis [49], graph-based analysis [50], and convolutional neural network [51] were suggested as methods that can discriminate MCI patients from HCs based on the fNIRS signal. These results indicate that fNIRS is a viable tool to detect the differences between MCI patients and HCs in the early stage of the disease.

The objective of this study is to propose a different feature extraction method from the literature, that is, a channel-specific classification. It is noted that the traditional feature extraction and classification methods have analyzed the time-domain characteristics of the averaged hemodynamic responses after extracting the ROI channels per task. However, in this paper, activation scores of all the channels per task are utilized as a feature. In this way, if we can narrow down the number of specific channels, the size of the entire fNIRS device can be reduced. Subsequently, using the proposed feature selection framework, we investigate whether fNIRS can distinguish patients with MCI from HCs according to task-relevant time-series hemodynamic signals. As cognitive tasks, a two-back task, a Stroop task, and a semantic verbal fluency task (SVFT) are examined. Activated brain regions are analyzed, and the features showing statistical between-group differences are extracted. Finally, linear discriminant analysis (LDA) is used to classify individuals into MCI and HC groups.

2. METHODS

2.1. Subjects

For this study, 15 patients with MCI were recruited from the Pusan National University Hospital, and 15 healthy peo-

ple participated as HCs, but 4 HCs were discarded due to experimental problems. No subjects had a history of cerebrovascular diseases or psychiatric disorders. Patients with MCI had been diagnosed by neurosurgery doctors, using the following three criteria: the Korean version of the MMSE (K-MMSE) [52], the Seoul Neuropsychological Screening Battery [53], and MRI data. The demographic information for all subjects is summarized in Table **1**, including age, sex, and K-MMSE scores. Before the experiment, each subject was fully informed about the purpose of the research and was asked to provide written informed consent. The entire experiment was approved by the Institute Review Board of Pusan National University Hospital and performed in accordance with the Declaration of Helsinki.

2.2. Equipment

A high-density fNIRS device (NIRSIT; OBELAB, Korea), which has 24 sources (laser diodes) and 32 detectors (a total of 204 channels, including short separations), was used to measure the hemodynamic responses in the prefrontal cortex at a sampling rate of 8.138 Hz. The NIRSIT is a wearable device that measures ΔHbO and ΔHbR, utilizing the difference in absorption rates of the near-infrared light through the cerebral cortex. To measure the concentration levels of two chromophores (ΔHbO and ΔHbR), two wavelengths (780 nm and 850 nm) were used. The distance between all sources and corresponding detectors was selected to be 3 cm, which resulted in a total of 48 channels from the prefrontal cortex (Fig. **1**). The NIRSIT and a tablet computer

Table 1. Demographic data for all subjects.

-	MCI (*n* = 15)	HC (n = 11)	*p*-Value[1]
Sex (male:female)	1:14	3:8	0.95
Age (range)	69.27 ± 7.09 (65~72)	69.09 ± 5.11 (65~75)	0.36
K-MMSE score	25.13 ± 2.33	27.22 ± 1.98	0.49

Abbreviations: MCI: mild cognitive impairment; HCs: healthy controls; K-MMSE: Korean Mini-Mental State Examination.
Note: [1]Two sample *t*-test.

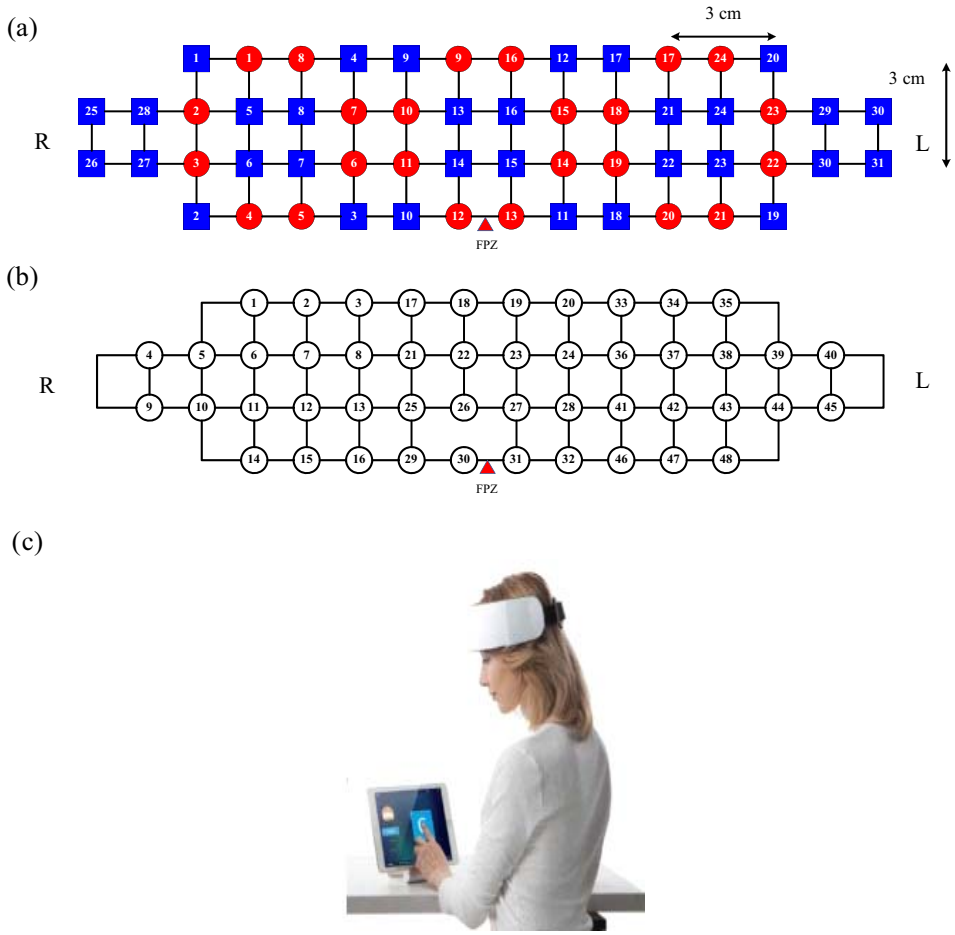

Fig. (1). The NIRSIT device: (**a**) Optodes configuration (red circles: sources; blue squares: detectors), (**b**) channel configurations, and (**c**) a photo illustrating how the NIRSIT is worn (https://fccid.io/2AHYINIRSIT/User-Manual/User-Manual-3032004). (*A higher resolution / colour version of this figure is available in the electronic copy of the article*).

(Galaxy Tab, Samsung, Republic of Korea) were connected via WLAN communication; the data were recorded on the tablet computer during the experiments.

2.3. Experimental Design

All subjects in both groups (HC, MCI) participated in three sessions, which consisted of three trials: two-back task, Stroop task, and SVFT. In the two-back task and Stroop task sessions, each trial was comprised of a 60 sec task period with a 30 sec rest period between tasks. Each SVFT trial consisted of three categories of words; each category block lasted for 20 sec, resulting in a total task period of 60 sec and followed by a 30 sec rest period. There was a 30 sec period before the trial started, which allowed participants to prepare for the SVFT. Before the two-back session, there was an initial resting time of 5 min (Fig. **2**). Experiment sessions consisted and applied to every subject in the same way.

The two-back task evaluates working memory. Words or numbers are presented, and the number of words (or numbers) remembered is taken as a measure of working memory. In this study, a two-back task was used, in which a number between one and nine was displayed on the monitor. Subjects were asked to press a keyboard key when the number presented was the same as that shown two trials ahead (Fig. **3a**).

The Stroop test is a widely used measure of executive function, mental control, and response flexibility. The Stroop task requires new reactions while suppressing the dominant response, such as letter reading conditions and color reading conditions. The Korean-Color Word Stroop Test (K-CWST) was used in the current study. Subjects were required to state the color of letters, which were written in red, blue, yellow, and black, within a limited period (Fig. **3b**).

The SVFT requires participants to generate as many words as possible related to a given semantic category within a limited time. The semantic categories were selected with enough words to say in 1 min such as 'food', 'animal', and 'what can be seen at the mountain'. The task measures how much information can be retrieved from the categorization and memory repository within 1 min (Fig. **3c**).

2.4. Preprocessing

fNIRS signals were processed using MATLAB™ (2017a, MathWorks, USA). The fNIRS raw data were converted to concentration changes of HbO and HbR using the modified Beer-Lambert's law [54]. A 5th order Butterworth band-pass filter was applied to remove physiological noise (cardiac noise ~1 Hz, respiration ~0.25 Hz, and Mayer signal ~0.1 Hz) and machine noise with a cut-off frequency range of 0.005 Hz ~ 0.1 Hz. Then, the data were segmented into individual trials. Baseline correction was performed for each subject by subtracting the mean resting-state data (60 sec before the two-back task onset) from the task data [55].

2.5. ROI Channel Selection

Verifying the region where cortical activation occurred for a given stimulus is of primary importance in fNIRS data analysis [56]. The desired hemodynamic response function (dHRF) in this paper was generated by convoluting the

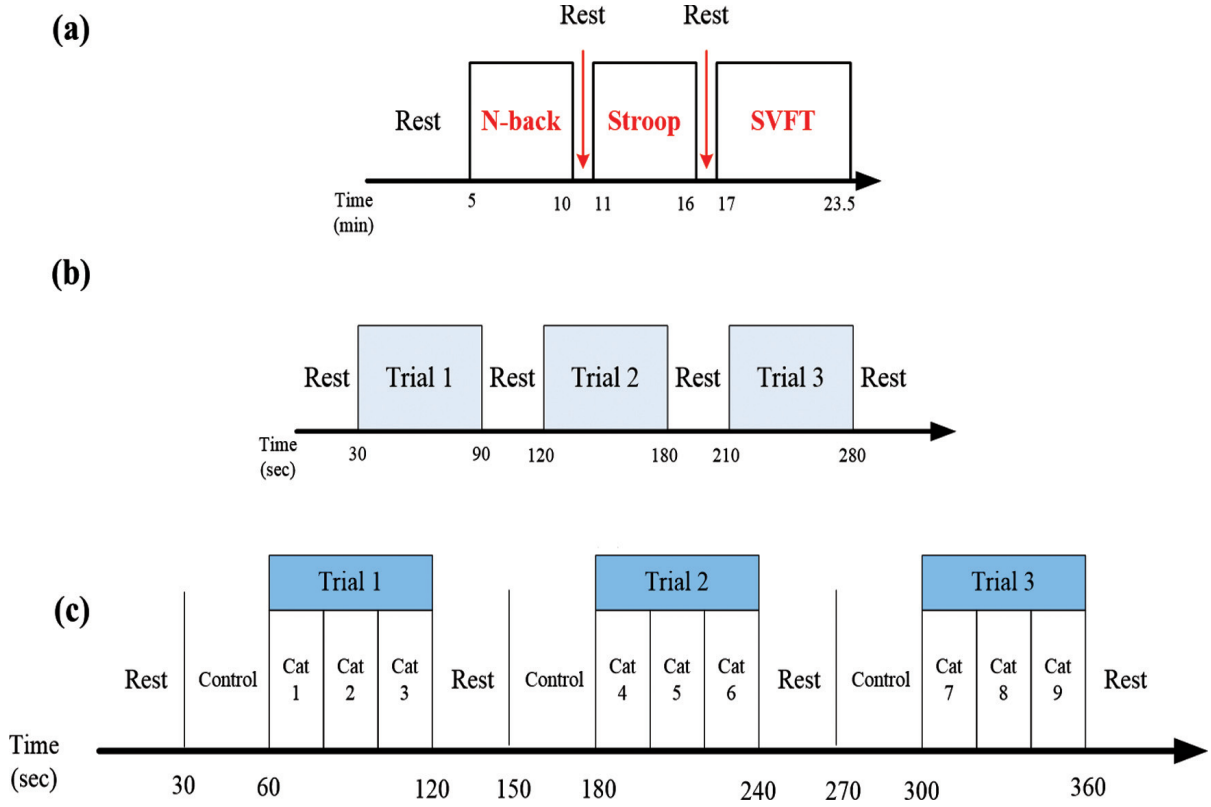

Fig. (2). Experimental paradigm: (**a**) One experiment including three sessions, (**b**) a session including three trials (two-back, Stroop), and (**c**) SVFT session showing three trials and three categories of words in each trial.

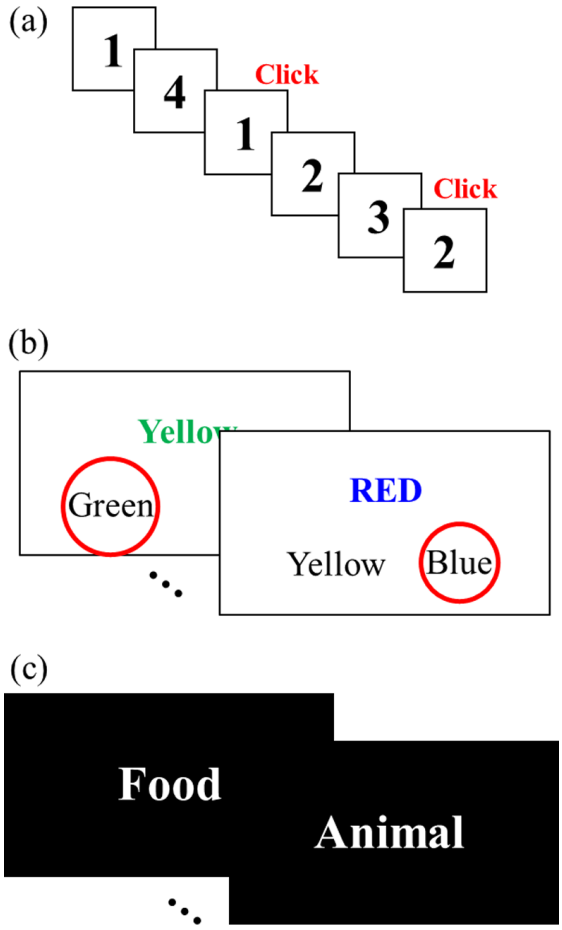

Fig. (3). Task contents: (**a**) two-back task, (**b**) Stroop task, and (**c**) semantic verbal fluency task. (*A higher resolution / colour version of this figure is available in the electronic copy of the article*).

stimulus pattern/period (*i.e.*, the period 60 sec task and 30 sec rest) with the canonical hemodynamic response function composed of two gamma functions [36]. The *t*-value is defined as the ratio of the weighting factor (when the measured data is fit linearly to the dHRF) and the standard error [57]. The meaning of the *t*-value in this work is conceptually the same as that in the fMRI field. A high *t*-value indicates that a signal is strongly correlated with the dHRF.

For each subject, the region of interest (ROI) was identified (for the three tasks), which indicates a brain region in which the *t*-value is higher than the critical *t*-value (t_{crt}). In this study, t_{crt} was set to 1.9632, which was calculated using the degree of freedom of the data and the level of statistical significance ($p < 0.05$ for two-sided tests) [36]. Fig. (**4**) compares the proposed method and the conventional one available in the literature. Conventionally (see the right-hand side in Fig. **4**), for a given task, the activated channels (*i.e.*, *t*-value > t_{crt}) for a trial are identified, which becomes the ROI channels. Subsequently, the ROI channels are averaged over all the trials and all the subjects (for the given task), resulting in the averaged HbOs for tasks. Then, features are extracted from the averaged HbOs. Finally, classification is performed using the extracted features.

In this paper, for a given task, the group analysis (between MCI and HC) for the channels showing the difference between the two groups is carried out first. It is noted that there exist 45 MCI data (*i.e.*, 3 trials × 15 subjects) and 33 HC data (*i.e.*, 3 trials × 11 HC subjects) per channel. To identify the activated channels for a task, the activated trial with a *t*-value higher than t_{crt} was assigned a value of 1, the deactivated trial with a *t*-value less than the $-t_{crt}$ was assigned a value of -1, and anything else was assigned a value of 0. For example, when all trials for a given channel are activated during the two-back task, the activation score of the channel becomes 3. To know whether a certain channel is activated or not, the activation scores between the two groups were tested using the two-sample *t*-test. Then, the channels whose *p*-value < 0.05 are identified as the ROI channels.

2.6. Feature Selection

Signals from each ROI were collected for further analysis in feature selection and classification. Using only the (unaveraged) signals from the relevant ROI improved classification accuracy. The features selected were the mean, slope, skewness, kurtosis, and peak value [58, 59]. The mean is the average hemodynamic response throughout the trial time window, which can distinguish the activation that occurs by comparing it with the resting state. The slope indicates the speed of activation. The slope was calculated by MATLAB™ function *polyfit*. The skewness is a measure of the asymmetry of a signal, and the kurtosis is a measure of the peakedness of the distribution. Most studies focused on the mean and peak of HbO to differentiate tasks, but we extracted various features that reflect prefrontal cortex activation from hemodynamic function's shape. The following equations were applied to calculate features:

$$mean = \frac{1}{N}\sum_{i=1}^{N} A_i \quad (1)$$

$$skewness = \frac{\frac{1}{N}\sum_{i=1}^{N}(A_i - mean)^3}{\sqrt{\frac{1}{N}\sum_{i=1}^{N}(A_i - mean)}^3} \quad (2)$$

$$kurtosis = \frac{\frac{1}{N}\sum_{i=1}^{N}(A_i - mean)^4}{\sqrt{\frac{1}{N}\sum_{i=1}^{N}(A_i - mean)}^4} \quad (3)$$

where N is the number of data of each trial, and A_i are the data points. The mean, slope, and skewness were used for the traditional method. For the proposed method, to verify ROI channels, the features were extracted from two types of ROI channels which were selected by the number of activated trials and *t*-values. Extracted features of ROI channels were divided into MCI and HC groups, and a two-sample *t*-test was performed. Features with *p*-values less than 0.05 were selected for classification.

2.7. Classification

Extracted features based on ROIs for 78 trials (26 subjects × 3 trials for each task) were classified by the LDA and SVM to distinguish between the MCI and HC groups. In this study, 10-fold cross-validation was used to assess the classification accuracy. The performance of the classifier was tested by receiver operating characteristic (ROC) analysis.

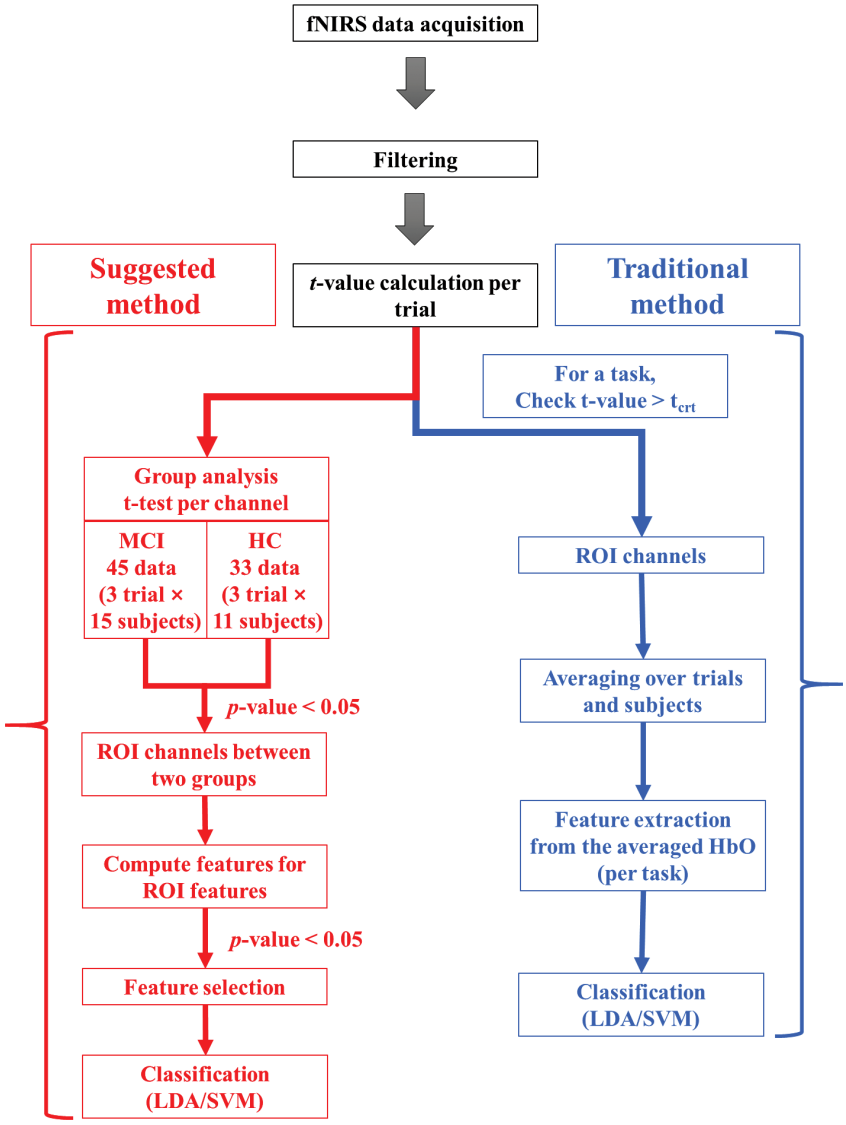

Fig. (4). Feature selection framework of the suggested method (red) and traditional method (blue). (*A higher resolution / colour version of this figure is available in the electronic copy of the article*).

3. RESULTS

3.1. ROI Channel Selection

To identify the activated channel within one task, the activated trial with a *t*-value higher than t_{crt} was assigned a value of 1. The deactivated trial with a *t*-value less than the -t_{crt} was assigned a value of -1. Anything else was assigned a value of 0. For example, when all trials of the channel were activated during the two-back task, the maximum number of activated trials for the channel was 3.

The number of activated trials of each channel and calculated *t*-values for each group during the two-back task are shown in Tables **2** and **3**, respectively. From these results, Chs. 2, 3, 4, 6, 7, 30, 33, and 39 were selected as ROIs. The hemodynamic signal was averaged for each group. MCI group's HbO of Ch.30 was strongly correlated with dHRF, but no such correlation was seen in that of the HC group. Based on calculated *t*-values, the brain activation map was plotted (Fig. **4**). As shown in Table **2**, Chs. 2, 3, 4, 6, 7, 30, 33, and 39 show varying activation levels between the two groups. In the activation map, the activation in the left and right ventrolateral PFC (VLPFC) was significantly higher in the HCs compared to the Ch.30 in the MCI patients. It can be explained that the function of VLPFC is not working enough in MCI patients.

During the Stroop task, the ROIs were chosen according to the results presented in Tables **4** and **5**. Chs. 2, 3, 4, 9, 14, 25, 30, 31, and 36 were selected as ROIs. The brain activation map is shown in Fig. (**5**), which shows that the activation of many channels was significantly different between the two groups.

Finally, the ROIs for the SVFT were selected according to the results shown in Tables **6** and **7**. Chs. 14, 36, 40, 47, and 48 were chosen as the ROIs in this task. The brain activation map using *t*-values is shown in Fig. (**6**); it shows that HbO was higher in the HC group compared with the MCI group.

Table 2. The number of activated trials in the two-back task.

-	MCI Group	HC Group	*p*-Value
Ch. 2	0.27 ± 2.31	1.00 ± 1.61	0.377
Ch. 3	-0.53 ± 1.68	0.91 ± 1.76	0.045*
Ch. 4	-0.53 ± 2.10	1.27 ± 0.90	0.014*
Ch. 6	-0.27 ± 1.79	1.64 ± 1.80	0.014*
Ch. 7	0.33 ± 2.13	1.45 ± 1.81	0.171
Ch. 30	1.33 ± 2.13	-0.54 ± 2.38	0.045*
Ch. 33	-0.60 ± 1.88	1.36 ± 1.29	0.007*
Ch. 39	-1.07 ± 2.05	0.09 ± 2.21	0.182

Note: (* indicates that $p < 0.05$).

Table 3. *t*-values in the two-back task.

-	MCI Group	HC Group	*p*-Value
Ch. 2	-2.01 ± 24.57	9.69 ± 17.50	0.022*
Ch. 3	-3.78 ± 20.55	8.20 ± 19.01	0.012*
Ch. 4	-1.69 ± 17.59	6.71 ± 18.81	0.047*
Ch. 6	-3.90 ± 19.66	9.26 ± 24.64	0.011*
Ch. 7	1.96 ± 24.45	12.99 ± 23.15	0.048*
Ch. 30	10.91 ± 22.46	0.27 ± 23.74	0.047*
Ch. 33	-4.98 ± 17.93	7.55 ± 18.95	0.004*
Ch. 39	-5.73 ± 17.48	3.61 ± 17.78	0.024*

Note: ($^*p < 0.05$).

Table 4. The number of activated trials in the Stroop task.

-	MCI Group	HC Group	*p*-Value
Ch. 2	-0.33 ± 2.06	0.36 ± 2.46	0.440
Ch. 3	-0.60 ± 2.20	0.82 ± 2.27	0.122
Ch. 4	-0.40 ± 2.13	0.64 ± 2.06	0.226
Ch. 9	1.20 ± 1.74	-0.73 ± 2.37	0.025*
Ch. 14	0.53 ± 2.26	1.36 ± 2.16	0.355
Ch. 25	0.40 ± 2.32	-1.82 ± 0.98	0.007*
Ch. 30	1.87 ± 1.55	-0.09 ± 2.47	0.020*
Ch. 31	1.93 ± 1.53	0.18 ± 2.48	0.036*
Ch. 36	0.07 ± 2.22	-1.45 ± 2.07	0.088

Note: ($^*p < 0.05$).

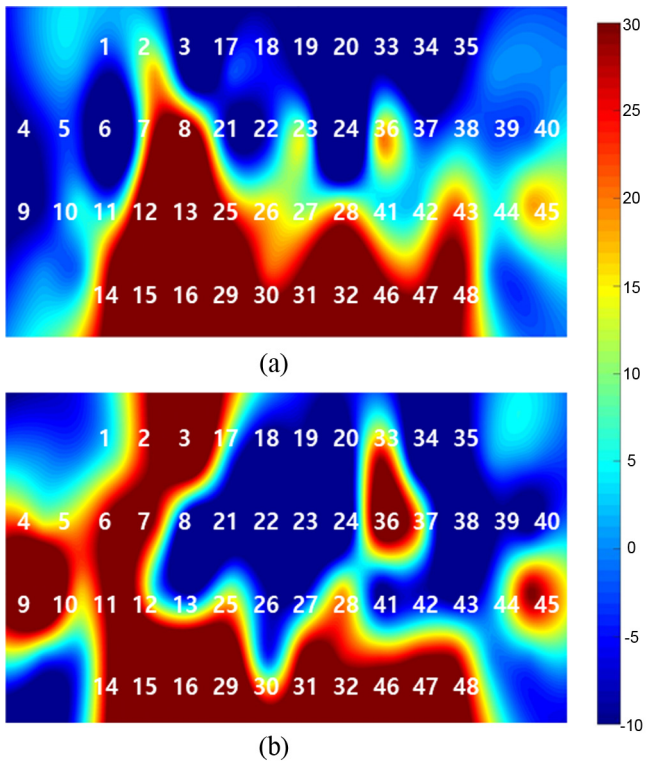

Fig. (5). Two-back task *t*-map: (**a**) MCI group, and (**b**) HC group. (*A higher resolution / colour version of this figure is available in the electronic copy of the article*).

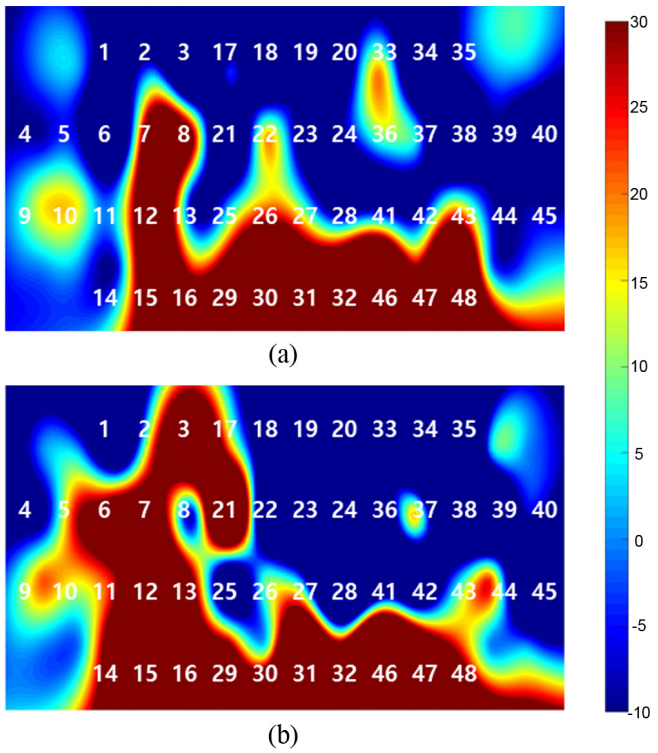

Fig. (6). Stroop task *t*-map: (**a**) MCI group, and (**b**) HC group. (*A higher resolution / colour version of this figure is available in the electronic copy of the article*).

Table 5. ***t*-values in the Stroop task.**

-	MCI Group	HC Group	*p*-Value
Ch. 2	-4.69 ± 18.89	9.26 ± 32.73	0.020*
Ch. 3	-8.55 ± 28.72	17.62 ± 36.51	0.001*
Ch. 4	-6.23 ± 24.23	11.81 ± 28.85	0.004*
Ch. 9	6.02 ± 18.08	1.23 ± 29.02	0.373
Ch. 14	1.54 ± 26.89	15.47 ± 33.82	0.046*
Ch. 25	-0.35 ± 25.07	-16.25 ± 27.55	0.010*
Ch. 30	23.10 ± 32.81	-0.07 ± 24.63	0.001*
Ch. 31	23.96 ± 33.85	9.39 ± 30.33	0.053
Ch. 36	0.69 ± 25.57	-16.76 ± 32.10	0.009*

Note: (*$p < 0.05$).

Table 6. **The number of activated trials in the semantic verbal fluency task.**

-	MCI Group	HC Group	*p*-Value
Ch. 14	0.53 ± 1.84	1.36 ± 1.91	0.275
Ch. 36	-0.2 ± 2.01	1.36 ± 1.57	0.042*
Ch. 40	-0.47 ± 2.03	1.64 ± 1.43	0.007*
Ch. 47	0.4 ± 2.35	2.09 ± 1.22	0.040*
Ch. 48	0.87 ± 2.42	3.18 ± 0.65	0.021*

Note: (*$p < 0.05$).

Table 7. *t*-values in the semantic verbal fluency task.

-	MCI Group	HC Group	*p*-Value
Ch. 14	2.03 ± 12.46	11.54 ± 22.00	0.018*
Ch. 36	-2.42 ± 21.44	5.57 ± 24.51	0.130
Ch. 40	-4.45 ± 22.13	14.06 ± 19.10	0.000*
Ch. 47	2.55 ± 18.93	12.78 ± 14.96	0.012*
Ch. 48	5.33 ± 19.05	16.94 ± 11.97	0.003*

Note: (*$p < 0.05$).

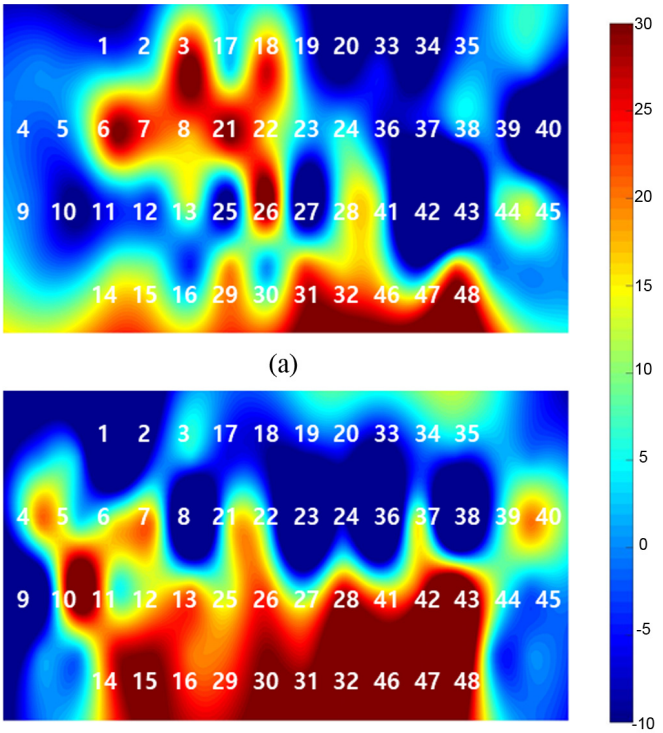

(a)

(b)

Fig. (7). SVFT *t*-map: (**a**) MCI group, and (**b**) HC group. (*A higher resolution / colour version of this figure is available in the electronic copy of the article*).

3.2. Feature Extraction

From the selected ROIs for each task, features (mean of HbO, mean of HbR, slope, skewness, kurtosis, and peak) were calculated. The *p*-values for features of the two groups were calculated using two-sample *t*-tests (Table **8**). For the two-back task, the peak of Ch. 4, the peak of Ch. 6, the peak of Ch. 7, and HbO mean of Ch. 7 were selected as features. For the Stroop task, the peak of Ch. 4, skewness of Ch. 30, kurtosis of Ch. 30, and skewness of Ch. 36 were used for classification. Finally, the skewness of Ch. 14, the slope of Ch. 36, the peak of Ch. 36, and HbO mean of Ch. 47 were selected for the SVFT. Fig. (**7**) shows the channels with the lowest *t*-values of features. For the SVFT, Ch. 30 of the HC group showed stronger activation than the MCI group (Fig. **7c**).

3.3. Classification

The classification accuracies of the traditional method have shown in Table **9**. For the two-back task, classification accuracies were 70.33% (LDA) and 66.67% (SVM). For the Stroop task, classification accuracies were 58.33% (LDA) and 62.5% (SVM). For the SVFT, classification accuracies were 75% (LDA) and 68.75% (SVM).

The extracted features by the suggested method were classified into MCI and HC groups (Table **10**). For the two-back task, classification accuracies were 64.10% (LDA) and 57.67% (SVM) for the peak of Ch. 7, 65.38% (LDA), and 67.95% (SVM) for the peaks of Ch. 4 and 7, and 69.23% (LDA) and 69.23 (SVM) for the peaks of Ch. 4 and 7 and HbO mean of Ch. 7. When combining all these features, the classification accuracy was 73.08% (LDA) and 69.23 (SVM). For the Stroop task, classification accuracies were 64.10% (LDA) and 71.79% (SVM) for the skewness of Ch. 30, 70.51% (LDA), and 75.64% (SVM) for the skewness of Ch. 30 and 36, 78.21% (LDA) and 70.51% (SVM) for the skewness of Ch. 30 and 36 and the peak of Ch. 4, and 79.49% (LDA) and 73.08% (SVM) for the skewness of Ch. 30 and 36, the peak of Ch. 4, and kurtosis of Ch. 30. Classification accuracy of the SVFT was 67.95% (LDA) and 64.10% (SVM) for the HbO mean of Ch. 47, 71.79% (LDA), and 73.08% (SVM) for the slope of Ch. 36 and HbO mean of Ch. 47, 79.49% (LDA) and 82.05% (SVM) for the slope and peak of Ch. 36 and HbO mean of Ch. 47, and 80.77% (LDA) and 83.33% (SVM) for the skewness of Ch. 14, slope and peak of Ch. 36, and HbO mean of Ch. 47.

To verify the classifier's performance, ROC analysis was performed for each classifier (Fig. **8**). For the two-back task, the area under the ROC curve (AUC) of LDA was 0.77, and the AUC of SVM was 0.91 when all four features were used. For the Stroop task, the AUC was 0.839 for LDA and 0.969 for SVM when all four features were used. The SVFT had the highest AUC of all three tasks, at 0.851 for LDA and 0.982 for SVM in the case of four channels.

4. DISCUSSIONS

4.1. Overview

In this study, through the variation of subject-wise and channel-specific hemodynamic signals using fNIRS, the ROIs were selected in the PFC for distinguishing MCI patients from HC. From the selected ROIs based on p-value,

Table 8. *p*-values of extracted features.

Two-Back Task						
-	**Mean (HbO)**	**Mean (HbR)**	**Slope**	**Skewness**	**Kurtosis**	**Peak**
Ch. 2	0.578	0.426	0.552	0.340	0.425	0.032*
Ch. 3	0.045*	0.480	0.195	0.595	0.979	0.453
Ch. 4	0.160	0.202	0.772	0.394	0.792	0.003*
Ch. 6	0.017*	0.173	0.822	0.177	0.537	0.010*
Ch. 7	0.008*	0.238	0.131	0.395	0.364	0.002*
Ch. 30	0.626	0.055	0.629	0.535	0.309	0.453
Ch. 33	0.821	0.276	0.429	0.157	0.262	0.053
Ch. 39	0.972	0.784	0.482	0.516	0.563	0.098
Stroop Task						
Ch. 2	0.101	0.544	0.863	0.562	0.680	0.062
Ch. 3	0.020*	0.558	0.099	0.419	0.080	0.383
Ch. 4	0.757	0.145	0.887	0.034*	0.213	0.000*
Ch. 9	0.612	0.301	0.236	0.853	0.195	0.002*
Ch. 14	0.038*	0.890	0.547	0.045*	0.878	0.020*
Ch. 25	0.845	0.609	0.174	0.029*	0.119	0.915
Ch. 30	0.063	0.009*	0.276	0.000*	0.018	0.842
Ch. 31	0.624	0.360	0.823	0.547	0.781	0.072
Ch. 36	0.907	0.480	0.128	0.000*	0.027*	0.710
Semantic Verbal Fluency Task						
Ch. 14	0.945	0.045*	0.325	0.002*	0.046*	0.356
Ch. 36	0.186	0.204	0.000*	0.966	0.720	0.001*
Ch. 40	0.135	0.064	0.149	0.197	0.548	0.017
Ch. 47	0.000*	0.016*	0.024*	0.512	0.013*	0.245
Ch. 48	0.490	0.528	0.557	0.313	0.567	0.594

Note: ($^{*}p < 0.05$).

Table 9. Classification accuracies of traditional method.

-	LDA	SVM
Two-back	70.33%	66.67%
Stroop	58.33%	62.5%
VFT	75%	68.75%

Table 10. Classification accuracies of suggested method.

-	# of Features	Two-Back (%)	Stroop (%)	SVFT (%)
LDA	1	64.10	64.10	67.95
	2	65.38	70.51	71.79
	3	69.23	78.21	79.49
	4	73.08	79.49	80.77
SVM	1	57.69	71.79	64.10
	2	67.95	75.64	73.08
	3	69.23	70.51	82.05
	4	69.23	73.08	83.33

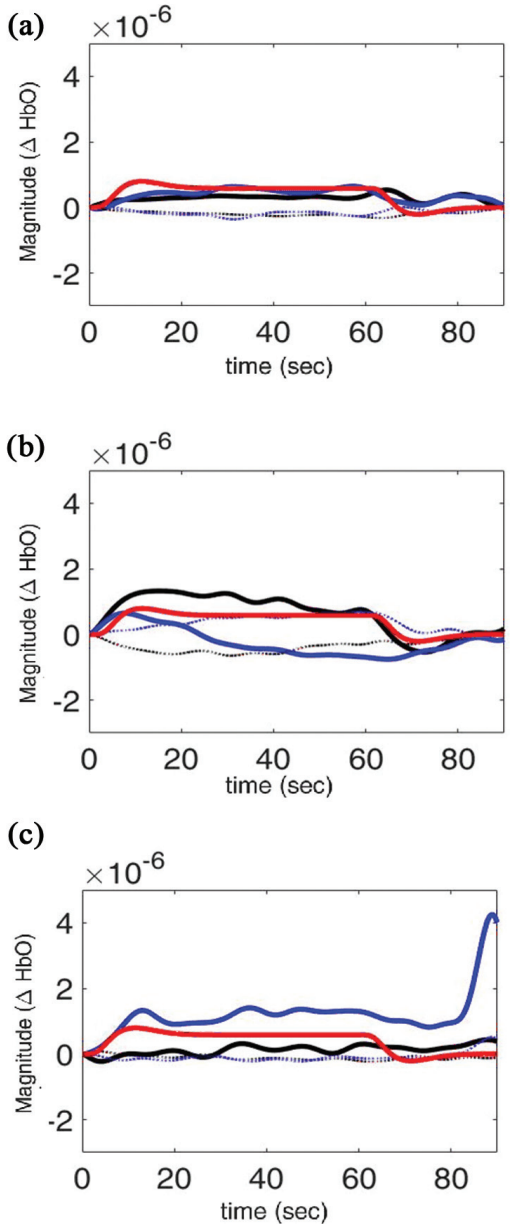

Fig. (8). Hemodynamic responses: (**a**) two-back task (Ch. 7), (**b**) Stroop task (Ch. 30), and (**c**) semantic verbal fluency task (Ch. 30) (red solid line: desired hemodynamic response function; black solid/dotted lines: HbO/HbR of a representative patient in the MCI group, respectively; blue solid/dotted lines: HbO/HbR of a representative patient in the HC group, respectively). (*A higher resolution / colour version of this figure is available in the electronic copy of the article*).

the graphical features were extracted for classification and achieved over 80% classification accuracies by LDA and SVM. Therefore, the results suggest the feature selection method has the possibility to enable the identification of MCI at an individual level.

4.2. ROIs Depending on the Tasks

First, during the two-back task, Chs. 2, 3, 4, 6, 7, 30, 33, and 39 have been selected as the ROIs. There are significantly higher brain activations in the HCs' ROIs except Ch. 30. The Chs. 2, 3, 4, 6, 7, 33, and 39 are located on the left and right ventrolateral prefrontal cortex (VLPFC), which is known for interpreting the meaning of the detection information and to signal which response to cancel or block, thereby facilitating decision-making on future responses [60]. Second, Chs. 2, 3, 4, 9, 14, 25, 30, 31, and 36 have been selected for the Stroop task. Specifically, Chs. 9, 30, 31, and 36 showed higher activation in the MCI than HC. In common with the two tasks, MCI patients showed higher brain activation in Ch 30. Finally, Chs. 14, 36, 40, 47, and 48 showed significantly high brain activation in HC during the SVFT (Fig. **9**).

Based on these results, the brain was activated differently between both groups during the same performing tasks. Also, our results showed that the MCI patients' decision making seems more difficult than HC because of dysfunction of PFC. MCI patients' HR was higher than HC in the Ch. 30 during the two-back and Stroop task. It might be caused by the dysfunction of VLPFC oxygen consumption which is higher than HC while performing the same tasks. Even though the magnitude of HR does not seem significantly different, the fluctuation of HR is higher in the MCI patients.

4.3. Classification

Classification of the hemodynamic signals according to a given task within subjects has primarily been studied using fNIRS. Distinguishing between different tasks using hemodynamic responses within one subject does not require consideration of different personal health conditions [61]. However, the discrimination of hemodynamic signals using fNIRS for the diagnosis of diseases should not overlook the complexity of and the individual differences in hemodynamic signals. The potential for fNIRS to be used for medical diagnosis has been investigated in the context of migraine [62], dementia [63], incremental swing balance task [64], attention-deficit/hyperactivity disorder [65, 66], psychosis, schizophrenia [67], and post-traumatic stress disorder [68]. Akin *et al*. [62] have researched that the hemodynamic changes during migraine which is hypothesized to be a neurovascular coupling disorder where the cerebral vascular reactivity is malfunctioning using fNIRS. For the diagnosis of attention-deficit/hyperactivity disorder, Ichikawa *et al*. [65] found that fNIRS had an 84% of classification accuracy from autism spectrum disorders, and Yukifumi *et al*. [66] classified individuals with attention-deficit/hyperactivity disorder from HCs with an AUC value of 0.85 and 90% sensitivity. According to the previous studies, our approach simplifies the process of selecting ROIs and features to not only account for subject-wise differences but also achieve a better performance of classifiers.

Several studies have investigated the ability of different imaging methods to distinguish patients with MCI from healthy controls. Ritchie *et al*. [69] evaluated the diagnostic criteria for MCI and reported an AUC of 0.485 using behavioral data. T1-weighted MRI-based classification has shown a 94% specificity, 73% sensitivity, and an AUC of 0.91 [70]. Another study reported specificity of over 85% and a sensitivity of 73% [71]. Multidimensional classification of hippocampal shape features has resulted in a classification accuracy of 83% [72]. Additionally, multimodal classification

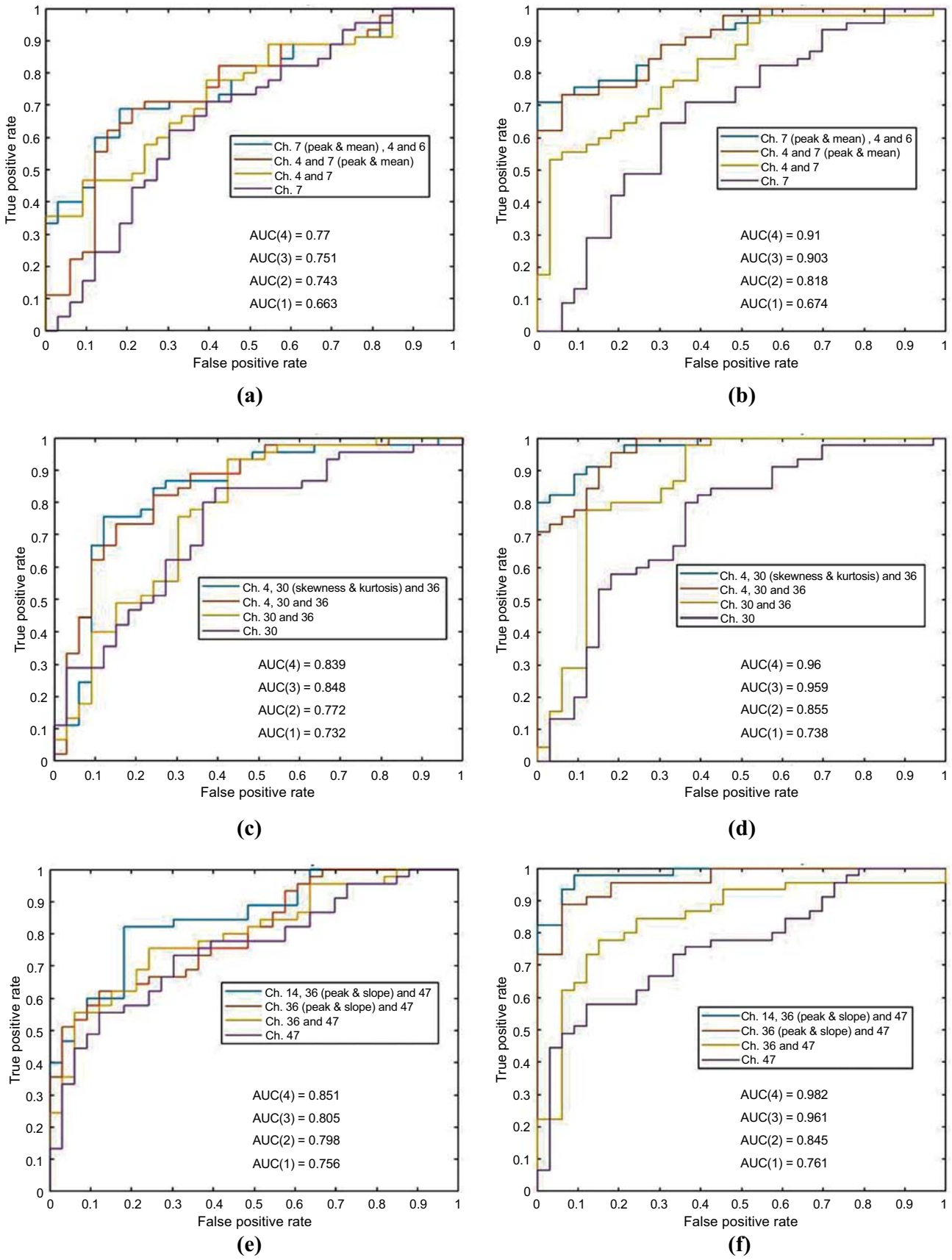

Fig. (9). ROC analysis of extracted features: (**a**) Two-back using LDA, (**b**) Two-back using SVM, (**c**) Stroop using LDA, (**d**) Stroop using SVM, (**e**) SVFT using LDA, (**f**) SVFT using SVM. (*A higher resolution / colour version of this figure is available in the electronic copy of the article*).

using multiple biomarkers (*i.e*., structural MRI, fluorodeoxyglucose-PET, and CSF analysis) showed a classification accuracy of 76.4% [73]. In this study, the classification accuracy was the highest in the case of the SVFT, at 83.33% with an AUC of 0.982 by SVM. Compared to these previous studies, our research has the limitation of having a smaller number of participants.

Selecting proper features is the most important step in achieving good performance in the classifier. In this paper, LDA and SVM are used as the classifier, which is the most basic classifier still used in various areas [74, 75]. Therefore, the use of classifiers like a neural network, which has recently been studied as showing better performance, could provide better performance with the same features [76, 77]. Also, nonetheless, the small number of subjects, our results have shown better performance than other studies. Although there is a limit to generalization due to a small number of subjects, considering the values of other methods reported in previous studies, our results show sufficient accuracy and reliability. This indicates that fNIRS can be used to diagnose MCI.

4.4. Future Work

During the revision process of the manuscript, one reviewer raised two interesting questions: i) whether two groups can be identified with the resting state fNIRS data, and ii) classification accuracy with the augmented data of three tasks. Out of 48-channel resting-state data before the two-back task, we were not able to find any statistical difference from the mean values between the two groups in the case of HbO. However, a statistical difference was found in the case of mean HbRs at two channels (*i.e*., Ch. 26, Ch. 33). Since the evidence is weak, our preliminary conclusion is that two groups cannot be distinguished from resting-state data. However, since the resting-state analysis is an interesting topic, it is left for our future research. Regarding the data augmentation of three tasks, the authors conjecture that if the data of three tasks are augmented in the classification process, the accuracy will be improved. However, this is also left for future research.

CONCLUSION

We individually evaluated the variation of subject-wise and channel-specific hemodynamic signals using fNIRS, which allowed us to select ROIs for each task successfully and to distinguish patients with MCI from HCs. The extracted features from the selected ROIs had an accuracy of 80.77% (LDA) and 83.33% (SVM) for the SVFT. In contrast, the conventional feature selection method had shown the 75% (LDA) and 68.75% (SVM). As a result, the proposed feature selection method showed better classification accuracy than the existing method. This was more pronounced in SVM than in LDA, apparently due to the reduction in the complexity of fNIRS data from the proposed method. Additionally, the classifier performance was validated with an AUC of 0.851 (LDA) and 0.982 (SVM). According to our results, this new fNIRS-based channel selection method could be an efficient diagnostic tool to identify MCI while considering individual differences in hemodynamics. However, future work should verify this conclusion using a larger sample size to compensate for our limitations, which were biased using the ROIs showing the most significant between-group differences. In addition, establishing an fNIRS system that has potential diagnostic applications will require future studies to address the limitations and to increase the classification accuracies up to 90%.

ETHICS APPROVAL AND CONSENT TO PARTICIPATE

The entire experiment was approved by the Institute Review Board of Pusan National University Hospital, Republic of Korea.

HUMAN AND ANIMAL RIGHTS

No animals were used in this research. All human experiments' procedures followed were in accordance with the standards set forth in the Declaration of Helsinki principles.

CONSENT FOR PUBLICATION

Patient consent of all participants was obtained.

AVAILABILITY OF DATA AND MATERIALS

Not applicable.

FUNDING

This work was funded by the Busan Institute of S&T Evaluation and Planning (BISTEP) and in part by the National Research Foundation (NRF) of Korea under the auspices of the Ministry of Science and ICT, Republic of Korea (Grant Nos. NRF-2017M3A9E9032772, NRF-2020R1A2B5B03096000).

CONFLICT OF INTEREST

The authors declare no conflict of interest, financial or otherwise.

ACKNOWLEDGEMENTS

This work was supported in part by the Open Laboratory Operational Business Developing and Diffusing the Regional Specialization Technology.

REFERENCES

[1] Karantzoulis S, Galvin JE. Distinguishing Alzheimer's disease from other major forms of dementia. Expert Rev Neurother 2011; 11(11): 1579-91.
http://dx.doi.org/10.1586/ern.11.155 PMID: 22014137

[2] Kumar A, Singh A, Ekavali. A review on Alzheimer's disease pathophysiology and its management: An update. Pharmacol Rep 2015; 67(2): 195-203.
http://dx.doi.org/10.1016/j.pharep.2014.09.004 PMID: 25712639

[3] 2018 Alzheimer's disease facts and figures. Alzheimers Dement 2018; 14(5): 701-1.

[4] Folch J, Petrov D, Ettcheto M, *et al.* Current research therapeutic strategies for Alzheimer's disease treatment. Neural Plast 2016; 2016: 8501693.
http://dx.doi.org/10.1155/2016/8501693 PMID: 26881137

[5] Gates NJ, Sachdev P. Is cognitive training an effective treatment for preclinical and early Alzheimer's disease? J Alzheimers Dis 2014; 42(4): S551-9.
http://dx.doi.org/10.3233/JAD-141302 PMID: 25171716

[6] Murphy MP, LeVine H III. Alzheimer's disease and the amyloid-beta peptide. J Alzheimers Dis 2010; 19(1): 311-23. http://dx.doi.org/10.3233/JAD-2010-1221 PMID: 20061647

[7] Rajmohan R, Reddy PH. Amyloid-beta and phosphorylated tau accumulations cause abnormalities at synapses of Alzheimer's disease neurons. J Alzheimers Dis 2017; 57(4): 975-99. http://dx.doi.org/10.3233/JAD-160612 PMID: 27567878

[8] Petersen RC, Smith GE, Waring SC, *et al*. Mild cognitive impairment: Clinical characterization and outcome. Arch Neurol 1999; 56(3): 303-8. http://dx.doi.org/10.1001/archneur.56.3.303 PMID: 10190820

[9] Petersen RC, Doody R, Kurz A, *et al.* Current concepts in mild cognitive impairment. Arch Neurol 2001; 58(12): 1985-92. http://dx.doi.org/10.1001/archneur.58.12.1985 PMID: 11735772

[10] Petersen RC. Mild cognitive impairment as a diagnostic entity. J Intern Med 2004; 256(3): 183-94. http://dx.doi.org/10.1111/j.1365-2796.2004.01388.x PMID: 15324362

[11] Tombaugh TN, McIntyre NJ. The mini-mental state examination: A comprehensive review. J Am Geriatr Soc 1992; 40(9): 922-35. http://dx.doi.org/10.1111/j.1532-5415.1992.tb01992.x PMID: 1512391

[12] Mattsson N, Andreasson U, Persson S, *et al.* The Alzheimer's association external quality control program for cerebrospinal fluid biomarkers. Alzheimers Dement 2011; 7(4): 386-395.e6. http://dx.doi.org/10.1016/j.jalz.2011.05.2243 PMID: 21784349

[13] Mattsson N, Andreasson U, Persson S, *et al.* CSF biomarker variability in the Alzheimer's Association quality control program. Alzheimers Dement 2013; 9(3): 251-61. http://dx.doi.org/10.1016/j.jalz.2013.01.010 PMID: 23622690

[14] Nho K, Kueider-Paisley A, MahmoudianDehkordi S, *et al.* Altered bile acid profile in mild cognitive impairment and Alzheimer's disease: Relationship to neuroimaging and CSF biomarkers. Alzheimers Dement 2019; 15(2): 232-44. http://dx.doi.org/10.1016/j.jalz.2018.08.012 PMID: 30337152

[15] Risacher SL, Saykin AJ, West JD, *et al*. Baseline MRI predictors of conversion from MCI to probable AD in the ADNI cohort. Curr Alzheimer Res 2009; 6(4): 347-61. http://dx.doi.org/10.2174/156720509788929273 PMID: 19689234

[16] Dubois B, Feldman HH, Jacova C, *et al.* Research criteria for the diagnosis of Alzheimer's disease: Revising the NINCDS-ADRDA criteria. Lancet Neurol 2007; 6(8): 734-46. http://dx.doi.org/10.1016/S1474-4422(07)70178-3 PMID: 17616482

[17] Bruña R, Poza J, Gómez C, García M, Fernández A, Hornero R. Analysis of spontaneous MEG activity in mild cognitive impairment and Alzheimer's disease using spectral entropies and statistical complexity measures. J Neural Eng 2012; 9(3): 036007 http://dx.doi.org/10.1088/1741-2560/9/3/036007 PMID: 22571870

[18] Poza J, Gómez C, García M, Corralejo R, Fernández A, Hornero R. Analysis of neural dynamics in mild cognitive impairment and Alzheimer's disease using wavelet turbulence. J Neural Eng 2014; 11(2): 026010. http://dx.doi.org/10.1088/1741-2560/11/2/026010 PMID: 24608272

[19] Jeong J. EEG dynamics in patients with Alzheimer's disease. Clin Neurophysiol 2004; 115(7): 1490-505. http://dx.doi.org/10.1016/j.clinph.2004.01.001 PMID: 15203050

[20] Liu J, Pan Y, Wu FX, Wang J. Enhancing the feature representation of multi-modal MRI data by combining multi-view information for MCI classification. Neurocomputing 2020; 400(4): 322-32. http://dx.doi.org/10.1016/j.neucom.2020.03.006

[21] Pihlajamäki M, Jauhiainen AM, Soininen H. Structural and functional MRI in mild cognitive impairment. Curr Alzheimer Res 2009; 6(2): 179-85. http://dx.doi.org/10.2174/156720509787602898 PMID: 19355853

[22] Li C, Zheng J, Wang J, Gui L, Li C. An fMRI stroop task study of prefrontal cortical function in normal aging, mild cognitive impairment, and Alzheimer's disease. Curr Alzheimer Res 2009; 6(6): 525-30. http://dx.doi.org/10.2174/156720509790147142 PMID: 19747163

[23] Li X, Zhu Z, Zhao W, *et al.* Decreased resting-state brain signal complexity in patients with mild cognitive impairment and Alzheimer's disease: A multiscale entropy analysis. Biomed Opt Express 2018; 9(4): 1916-29. http://dx.doi.org/10.1364/BOE.9.001916 PMID: 29675329

[24] Sasaki S. High prevalence of parkinsonism in patients with MCI or mild Alzheimer's disease. Alzheimers Dement 2018; 14(12): 1615-22. http://dx.doi.org/10.1016/j.jalz.2018.06.3054 PMID: 30222946

[25] Klunk WE, Engler H, Nordberg A, *et al.* Imaging brain amyloid in Alzheimer's disease with Pittsburgh Compound-B. Ann Neurol 2004; 55(3): 306-19. http://dx.doi.org/10.1002/ana.20009 PMID: 14991808

[26] Mintun MA, Larossa GN, Sheline YI, *et al.* [11C]PIB in a nondemented population: Potential antecedent marker of Alzheimer disease. Neurology 2006; 67(3): 446-52. http://dx.doi.org/10.1212/01.wnl.0000228230.26044.a4 PMID: 16894106

[27] Jack CR Jr, Knopman DS, Jagust WJ, *et al.* Hypothetical model of dynamic biomarkers of the Alzheimer's pathological cascade. Lancet Neurol 2010; 9(1): 119-28. http://dx.doi.org/10.1016/S1474-4422(09)70299-6 PMID: 20083042

[28] Albert MS, DeKosky ST, Dickson D, *et al.* The diagnosis of mild cognitive impairment due to Alzheimer's disease: Recommendations from the National Institute on Aging-Alzheimer's Association workgroups on diagnostic guidelines for Alzheimer's disease. Alzheimers Dement 2011; 7(3): 270-9. http://dx.doi.org/10.1016/j.jalz.2011.03.008 PMID: 21514249

[29] Villemagne VL, Burnham S, Bourgeat P, *et al.* Amyloid β deposition, neurodegeneration, and cognitive decline in sporadic Alzheimer's disease: A prospective cohort study. Lancet Neurol 2013; 12(4): 357-67. http://dx.doi.org/10.1016/S1474-4422(13)70044-9 PMID: 23477989

[30] Afrasiabi M, Noroozian N. Advantages and limitations of functional magnetic resonance imaging (fMRI) of the human visual brain. In: Costa A, Villalba E, Eds. Horizons in Neuroscience Research. New York: Nova Science Publishers 2015; pp. 65-72.

[31] Poza J, Gómez C, García M, *et al.* Spatio-temporal fluctuations of neural dynamics in mild cognitive impairment and Alzheimer's disease. Curr Alzheimer Res 2017; 14(9): 924-36. http://dx.doi.org/10.2174/1567205014666170309115656 PMID: 28290246

[32] Stam CJ, Jones BF, Nolte G, Breakspear M, Scheltens P. Small-world networks and functional connectivity in Alzheimer's disease. Cereb Cortex 2007; 17(1): 92-9. http://dx.doi.org/10.1093/cercor/bhj127 PMID: 16452642

[33] Gallego-Jutglà E, Solé-Casals J, Vialatte FB, Elgendi M, Cichocki A, Dauwels J. A hybrid feature selection approach for the early diagnosis of Alzheimer's disease. J Neural Eng 2015; 12(1): 016018. http://dx.doi.org/10.1088/1741-2560/12/1/016018 PMID: 25605667

[34] Waldemar G, Dubois B, Emre M, *et al.* Recommendations for the diagnosis and management of Alzheimer's disease and other disorders associated with dementia: EFNS guideline. Eur J Neurol 2007; 14(1): e1-e26. http://dx.doi.org/10.1111/j.1468-1331.2006.01605.x PMID: 17222085

[35] Stuart S, Vitorio R, Morris R, Martini DN, Fino PC, Mancini M. Cortical activity during walking and balance tasks in older adults and in people with Parkinson's disease: A structured review. Maturitas 2018; 113: 53-72. http://dx.doi.org/10.1016/j.maturitas.2018.04.011 PMID: 29903649

[36] Naseer N, Hong KS. FNIRS-based brain-computer interfaces: A review. Front Hum Neurosci 2015; 9(3): 1-15.

[37] Nguyen HD, Hong KS. Bundled-optode implementation for 3D imaging in functional near-infrared spectroscopy. Biomed Opt Express 2016; 7(9): 3491-507. http://dx.doi.org/10.1364/BOE.7.003491 PMID: 27699115

[38] Ghafoor U, Lee JH, Hong KS, Park SS, Kim J, Yoo HR. Effects of acupuncture therapy on MCI patients using functional near-infrared spectroscopy. Front Aging Neurosci 2019; 11(237): 237. http://dx.doi.org/10.3389/fnagi.2019.00237 PMID: 31543811

[39] Yap KH, Ung WC, Ebenezer EGM, *et al.* Visualizing hyperactivation in neurodegeneration based on prefrontal oxygenation: A comparative study of mild Alzheimer's disease, mild cognitive impairment, and healthy controls. Front Aging Neurosci 2017; 9(287): 287. http://dx.doi.org/10.3389/fnagi.2017.00287 PMID: 28919856

[40] Li R, Rui G, Chen W, Li S, Schulz PE, Zhang Y. Early detection of Alzheimer's disease using non-invasive near-infrared spectroscopy. Front Aging Neurosci 2018; 10: 366. http://dx.doi.org/10.3389/fnagi.2018.00366 PMID: 30473662

[41] Vermeij A, Kessels RPC, Heskamp L, Simons EMF, Dautzenberg PLJ, Claassen JAHR. Prefrontal activation may predict working-memory training gain in normal aging and mild cognitive impairment. Brain Imaging Behav 2017; 11(1): 141-54. http://dx.doi.org/10.1007/s11682-016-9508-7 PMID: 26843001

[42] Nguyen T, Kim M, Gwak J, *et al.* Investigation of brain functional connectivity in patients with mild cognitive impairment: A functional near-infrared spectroscopy (fNIRS) study. J Biophotonics 2019; 12(9): e201800298.
http://dx.doi.org/10.1002/jbio.201800298 PMID: 30963713

[43] Yoon JA, Kong IJ, Choi J, *et al.* Neural compensatory response during complex cognitive function tasks in mild cognitive impariment: A near-infrared spectroscopy study. Neural Plast 2019; 2019: 7845104.
http://dx.doi.org/10.1155/2019/7845104 PMID: 31320893

[44] Basso Moro S, Cutini S, Ursini ML, Ferrari M, Quaresima V. Prefrontal cortex activation during story encoding/retrieval: A multi-channel functional near-infrared spectroscopy study. Front Hum Neurosci 2013; 7(925): 925.
http://dx.doi.org/10.3389/fnhum.2013.00925 PMID: 24427131

[45] Jahani S, Fantana AL, Harper D, *et al.* fNIRS can robustly measure brain activity during memory encoding and retrieval in healthy subjects. Sci Rep 2017; 7(1): 9533.
http://dx.doi.org/10.1038/s41598-017-09868-w PMID: 28842618

[46] Skau S, Bunketorp-Käll L, Kuhn HG, Johansson B. Mental fatigue and functional near-infrared spectroscopy (fNIRS) - based assessment of cognitive performance after mild traumatic brain injury. Front Hum Neurosci 2019; 13(145): 145.
http://dx.doi.org/10.3389/fnhum.2019.00145 PMID: 31139065

[47] Heinzel S, Metzger FG, Ehlis AC, *et al.* Age and vascular burden determinants of cortical hemodynamics underlying verbal fluency. PLoS One 2015; 10(9): e0138863.
http://dx.doi.org/10.1371/journal.pone.0138863 PMID: 26394050

[48] Katzorke A, Zeller JBM, Müller LD, *et al.* Reduced activity in the right inferior frontal gyrus in elderly APOE-E4 carriers during a verbal fluency task. Front Hum Neurosci 2017; 11(46): 46.
http://dx.doi.org/10.3389/fnhum.2017.00046 PMID: 28220068

[49] Bu L, Huo C, Qin Y, Xu G, Wang Y, Li Z. Effective connectivity in subjects with mild cognitive impairment as assessed using functional near-infrared spectroscopy. Am J Phys Med Rehabil 2019; 98(6): 438-45.
http://dx.doi.org/10.1097/PHM.0000000000001118 PMID: 30557156

[50] Li R, Rui G, Zhao C, Wang C, Fang F, Zhang Y. Functional network alterations in patients with amnestic mild cognitive impairment characterized using functional near-infrared spectroscopy. IEEE Trans Neural Syst Rehabil Eng 2020; 28(1): 123-32.
http://dx.doi.org/10.1109/TNSRE.2019.2956464 PMID: 31804939

[51] Yang D, Hong KS, Yoo SH, Kim CS. Evaluation of neural degeneration biomarkers in the prefrontal cortex for early identification of patients with mild cognitive impairment: an fNIRS study. Front Hum Neurosci 2019; 13(317): 317.
http://dx.doi.org/10.3389/fnhum.2019.00317 PMID: 31551741

[52] Cho B, Yang J, Kim S, Yang DW, Park M, Chey J. The validity and reliability of a computerized dementia screening test developed in Korea. J Neurol Sci 2002; 203-204: 109-14.
http://dx.doi.org/10.1016/S0022-510X(02)00263-0 PMID: 12417367

[53] Ahn HJ, Chin J, Park A, *et al.* Seoul Neuropsychological Screening Battery-dementia version (SNSB-D): A useful tool for assessing and monitoring cognitive impairments in dementia patients. J Korean Med Sci 2010; 25(7): 1071-6.
http://dx.doi.org/10.3346/jkms.2010.25.7.1071 PMID: 20592901

[54] Hiraoka M, Firbank M, Essenpreis M, *et al.* A Monte Carlo investigation of optical pathlength in inhomogeneous tissue and its application to near-infrared spectroscopy. Phys Med Biol 1993; 38(12): 1859-76.
http://dx.doi.org/10.1088/0031-9155/38/12/011 PMID: 8108489

[55] Hong KS, Khan MJ, Hong MJ. Feature extraction and classification methods for hybrid fNIRS-EEG brain-computer interfaces. Front Hum Neurosci 2018; 12(246): 246.
http://dx.doi.org/10.3389/fnhum.2018.00246 PMID: 30002623

[56] Hong KS, Nguyen HD. State-space models of impulse hemodynamic responses over motor, somatosensory, and visual cortices. Biomed Opt Express 2014; 5(6): 1778-98.
http://dx.doi.org/10.1364/BOE.5.001778 PMID: 24940540

[57] Tak S, Kempny AM, Friston KJ, Leff AP, Penny WD. Dynamic causal modelling for functional near-infrared spectroscopy. Neuroimage 2015; 111: 338-49.
http://dx.doi.org/10.1016/j.neuroimage.2015.02.035 PMID: 25724757

[58] Yang D, Huang R, Yoo SH, *et al.* Detection of mild cognitive impairment using convolutional neural network: Temporal-feature maps of functional near-infrared spectroscopy. Front Aging Neurosci 2020; 12: 141.
http://dx.doi.org/10.3389/fnagi.2020.00141 PMID: 32508627

[59] De A, Bhattacharjee B, Konar A, Ralescu AL, Nagar AK. A type-2 fuzzy set induced classification of cognitive load in inter-individual working memory performance based on hemodynamic response. 2017 IEEE Symposium Series on Computational Intelligence (SSCI). 2017 Nov 27- Dec 1; Honolulu, HI, USA; Piscataway, NJ, USA: IEEE 1-7.
http://dx.doi.org/10.1109/SSCI.2017.8285186

[60] Sakagami M, Pan X. Functional role of the ventrolateral prefrontal cortex in decision making. Curr Opin Neurobiol 2007; 17(2): 228-33.
http://dx.doi.org/10.1016/j.conb.2007.02.008 PMID: 17350248

[61] Hong KS, Yaqub MA. Application of functional near-infrared spectroscopy in the healthcare industry: A review. J Innov Opt Health Sci 2019; 12(6): 1930012.
http://dx.doi.org/10.1142/S179354581930012X

[62] Akin A, Bilensoy D, Emir UE, Gülsoy M, Candansayar S, Bolay H. Cerebrovascular dynamics in patients with migraine: Near-infrared spectroscopy study. Neurosci Lett 2006; 400(1-2): 86-91.
http://dx.doi.org/10.1016/j.neulet.2006.02.016 PMID: 16516381

[63] Lech GM. Using functional near-infrared spectroscopy to measure cognitive function: when will it become an accepted clinical tool for cognitive aging and prodromal dementia screening? J Innov Opt Health Sci 2011; 4(4): 373-83.
http://dx.doi.org/10.1142/S179354581100171X

[64] Basso Moro S, Bisconti S, Muthalib M, *et al.* A semi-immersive virtual reality incremental swing balance task activates prefrontal cortex: A functional near-infrared spectroscopy study. Neuroimage 2014; 85(Pt 1): 451-60.
http://dx.doi.org/10.1016/j.neuroimage.2013.05.031 PMID: 23684867

[65] Ichikawa H, Kitazono J, Nagata K, *et al.* Novel method to classify hemodynamic response obtained using multi-channel fNIRS measurements into two groups: Exploring the combinations of channels. Front Hum Neurosci 2014; 8(480): 480.
http://dx.doi.org/10.3389/fnhum.2014.00480 PMID: 25071510

[66] Monden Y, Dan I, Nagashima M, *et al.* Individual classification of ADHD children by right prefrontal hemodynamic responses during a go/no-go task as assessed by fNIRS. Neuroimage Clin 2015; 9: 1-12.
http://dx.doi.org/10.1016/j.nicl.2015.06.011 PMID: 26266096

[67] Koike S, Satomura Y, Kawasaki S, *et al.* Application of functional near infrared spectroscopy as supplementary examination for diagnosis of clinical stages of psychosis spectrum. Psychiatry Clin Neurosci 2017; 71(12): 794-806.
http://dx.doi.org/10.1111/pcn.12551 PMID: 28692185

[68] Gramlich MA, Neer SM, Beidel DC, Bohil CJ, Bowers CA. A functional near-infrared spectroscopy study of trauma-related auditory and olfactory cues: Posttraumatic stress disorder or combat experience? J Trauma Stress 2017; 30(6): 656-65.
http://dx.doi.org/10.1002/jts.22239 PMID: 29160560

[69] Ritchie K, Artero S, Touchon J. Classification criteria for mild cognitive impairment: A population-based validation study. Neurology 2001; 56(1): 37-42.
http://dx.doi.org/10.1212/WNL.56.1.37 PMID: 11148233

[70] Desikan RS, Cabral HJ, Hess CP, *et al.* Automated MRI measures identify individuals with mild cognitive impairment and Alzheimer's disease. Brain 2009; 132(Pt 8): 2048-57.
http://dx.doi.org/10.1093/brain/awp123 PMID: 19460794

[71] Cuingnet R, Gerardin E, Tessieras J, *et al.* Automatic classification of patients with Alzheimer's disease from structural MRI: A comparison of ten methods using the ADNI database. Neuroimage 2011; 56(2): 766-81.
http://dx.doi.org/10.1016/j.neuroimage.2010.06.013 PMID: 20542124

[72] Gerardin E, Chételat G, Chupin M, *et al.* Multidimensional classification of hippocampal shape features discriminates Alzheimer's disease and mild cognitive impairment from normal aging. Neuroimage 2009; 47(4): 1476-86.
http://dx.doi.org/10.1016/j.neuroimage.2009.05.036 PMID: 19463957

[73] Zhang D, Wang Y, Zhou L, Yuan H, Shen D, Alzheimers Dis Neuroimaging I. Multimodal classification of Alzheimer's disease and mild cognitive impairment. Neuroimage 2011; 55(3): 856-67.
http://dx.doi.org/10.1016/j.neuroimage.2011.01.008 PMID: 21236349

[74] Moon IC, Song K, Kim SH, Choi HL. State prediction of high-speed ballistic vehicles with gaussian process. Int J Control Autom Syst 2018; 16(3): 1282-92.
http://dx.doi.org/10.1007/s12555-016-0552-2

[75] Kim TY, Kim BS, Park TC, Yeo YK. Development of predictive model based control scheme for a molten carbonate fuel cell (MCFC) process. Int J Control Autom Syst 2018; 16(2): 791-803.
http://dx.doi.org/10.1007/s12555-016-0234-0

[76] Moon J, Kim H, Lee B. View-point invariant 3D classification for mobile robots using a convolutional neural network. Int J Control Autom Syst 2018; 16(6): 2888-95.
http://dx.doi.org/10.1007/s12555-018-0182-y

[77] Zheng W, Wang HB, Zhang ZM, Li N, Yin PH. Multi-layer feed-forward neural network deep learning control with hybrid position and virtual-force algorithm for mobile robot obstacle avoidance. Int J Control Autom Syst 2019; 17(4): 1007-18.
http://dx.doi.org/10.1007/s12555-018-0140-8